Shock Temperatures in Anorthite Glass

Mark B. Boslough and Thomas J. Ahrens

Seismological Laboratory, California Institute of Technology, Pasadena, California 91125

Arthur C. Mitchell

Lawrence Livermore National Laboratory, Livermore, California 94550

ABSTRACT

Temperatures of $CaAl_2Si_2O_8$ (anorthite glass) shocked to pressures between 48 and 117 GPa have been measured in the range from 2500 to 5600 K, using optical pyrometry techniques. The pressure dependence of the shock temperatures deviates significantly from predictions based on a single high-pressure phase. At least three phase transitions, at pressures of about 55, 85, and 100 GPa and with transition energies of about 0.5 MJ/kg each ($\approx$1.5 MJ/kg total) are required to explain the shock-temperature data. The phase transition at 100 GPa can possibly be identified with the stishovite melting transition. Theoretical models of the time dependence of the thermal radiation from the shocked anorthite based on the geometry of the experiment and the absorptive properties of the shocked material yields good agreement with observations, indicating that it is not necessary to invoke intrinsic time dependences to explain the data in many cases. Observed time dependences were used to calculate absorption coefficient of the shocked material of from about 2 to >24 mm^{-1}— an increasing function of shock pressure. The assumption that the shocked material radiates as a blackbody is supported by

the theoretical model, and by the close agreement between measured and calculated blackbody spectral radiance as a function of wavelength.

Introduction

Because of the cosmochemical abundance of Ca and Al, and the refractory nature of calcium-aluminum silicates such as anorthite, their high pressure polymorphs are important to consider in any model of the earth's mantle. Models for the earth's composition based on chondritic abundances predict atomic abundance ratios of $\frac{Ca}{Si} \approx 0.05$ and $\frac{Al}{Si} \approx 0.07$ (Ross & Aller, 1976). It is possible, however, that the lower mantle is significantly enriched relative to the whole earth in calcium-aluminum silicates, because these are among the first phases to condense from the solar nebula (Grossman & Larimer, 1974) and accrete onto the earth, in inhomogeneous accretion models (Turekian & Clark, 1969). Moreover, the construction of equations of state for anorthosite are key ingredients in carrying out cratering calculations for impacts on the crusts of terrestrial planets (Ahrens & O'Keefe, 1977, 1982), and in determining quantities of melting and vaporization resulting from such an impact (Boslough & Ahrens, 1983).

In previous work on anorthite, a high pressure equation of state to pressures greater than 120 GPa has been constructed by Jeanloz & Ahrens (1980) based on Hugoniot data only. This equation of state is incomplete in that the thermal behavior of the shocked material was inferred from pressure-density states only. The parameter which is most sensitive to thermal properties and energetics of phase transitions, namely the temperature, was not measured.

Past work (Kormer *et al.*, 1965, Ahrens *et al.*, 1982, Lyzenga *et al.*, 1983, Boslough *et al.*, 1983a) has demonstrated the usefulness of shock-temperature data in constraining the high-pressure-high-temperature properties of materials, and in defining phase transitions. For example, the stishovite melting curve was determined from shock-temperature data on α-quartz and fused quartz. This phase transition is readily apparent from the temperature data, but is not at all obvious from Hugoniot data in the pressure-density plane (Lyzenga *et al.*, 1983). It is reasonable to expect similar results for other materials. The purpose of the present study was to measure temperatures of shocked anorthite glass using the optical pyrometry technique, and determine the high-pressure thermal behavior of $CaAl_2Si_2O_8$.

Experimental

Amorphous $CaAl_2Si_2O_8$ samples, with measured Archimedean initial densities of 2.69 Mg/m^3 were used in these shock-temperature experiments. The samples, obtained from Corning Glass Co. (Corning, N.Y.), were clear and homogeneous, with a composition described by $An_{99.5} Ab_{0.4} Or_{0.1}$ — essentially the composition of pure anorthite. A microprobe analysis of a representative sample is given in terms of oxides in Table 1. The transmittance of a 3mm thick, polished sample of the glass over the wavelength range of interest is shown in Fig. 1, measured with a Cary Model 17 spectrophotometer.

Shock experiments were carried out on two-stage light-gas guns at the California Institute of Technology and Lawrence Livermore National Laboratory. Copper and tantalum projectiles were accelerated to velocities between 3.7 and 5.7 km/s. Projectile velocities were determined using flash X-radiography, as described elsewhere (Jeanloz & Ahrens, 1977; Mitchell & Nellis, 1981). Shock pressures were determined by the method of impedance matching (Rice *et al.*,

1958) and using the standard equation of state of McQueen *et al.* (1970) for tantalum and copper, and the Hugoniot of Boslough *et al.* (1984), for the anorthite glass.

Temperatures were determined by measuring the intensity of thermally radiated light at several wavelengths in the visible and near infrared wavelengths. The thermal radiation was filtered by interference filters and focused onto silicon photodiodes. The resulting electrical signals were recorded by an array of oscilloscopes with Polaroid cameras. The recorded time-resolved voltages are directly proportional to the spectral radiances of the thermal radiation. Calibration of the pyrometer system was carried out using light sources with known spectral radiances in the wavelength range in which measurements were made. The two optical pyrometers used in this study are described in detail by Lyzenga & Ahrens (1979) and Boslough (1983).

Results

Eight shock-temperature experiments were conducted on anorthite glass; three using a 10 nm bandwidth six-channel optical pyrometer at Lawrence Livermore National Laboratory (Lyzenga & Ahrens, 1979), and five using a 40 nm bandwidth four-channel optical pyrometer at the California Institute of Technology (Boslough, 1983). Representative data are shown in Figs. 2 and 3.

Three general types of time-dependence were observed. In shots An6T, An5T, and An3T—the three experiments below 70 GPa--the sharp increase in intensity corresponding to the entrance of the shock wave into the sample is followed by an exponential decay to an approximately constant value (Fig. 2a). In shots An2T, An7T, An1T, and An10T--four experiments above 89 GPa--the light intensity remains constant to within about 10% until the shock wave reaches the free surface or is overtaken by an edge rarefaction (Fig. 2b). Shot An9T--to

about 85 GPa—shows an anomalous behavior, in which the intensity decreases at a nonuniform rate during shot transit (Fig. 3).

There are three causes which could account for time dependence in the emitted light: temperature dependence, emissivity dependences, or time dependence of the absorption or scattering of an intervening layer. All three of these causes are invoked to explain the observed time dependences. It is important to note that the observed light is not necessarily radiated from only the shock front unless the shocked material is perfectly opaque. In general, a material that is initially semi-transparent, with initial linear absorption coefficient a_u is shocked to a state with linear absorption coefficient a_s and temperature T. The absorbance of the unshocked layer is $A_u = e^{-a_u d_u}$, and the shocked layer is $A_s = e^{-a_s d_s}$, where d_n and d_s are the thicknesses of unshocked and shocked layers, respectively. According to Kirchoff's radiation law for a non-reflector (Jenkins & White, 1976) the emissivity of a layer is equal to its absorbance. If the sample thickness is d, the shock velocity is U_s, the velocity of the shocked material (particle velocity) is u_p, and graybody light (with a Planckian wavelength distribution and an emissivity less than unity) is radiated only from the shocked layer at constant temperature T, the time, t, dependence will be

$$I_s(t) = f_\lambda(T) \left[1 - e^{-a_s(U_s - u_p)t}\right] e^{-a_u(d - U_s t)}, \tag{1}$$

where $f_\lambda(T)$ is the Planck distribution function. In the case of anorthite glass, the initial state is essentially transparent (Fig. 1), so $a_u = 0$ and this becomes:

$$I_s(t) = f_\lambda(T) \left[1 - e^{-a_s(U_s - u_p)t}\right]. \tag{2}$$

It is also necessary to consider the effect of light generated at the interface between the driver and sample material, due to the non-ideality of the surfaces,

which, despite their optical quality, have imperfections which leave a gap on the order of 1μm wide as determined by counting visible fringes (Newton rings) with an optical flat.

The temperature at the interface due to passage of the shock wave is higher than the shock temperature of either boundary material, due to multiple reverberation (Urtiew & Grover, 1974) and shock heating of any gas trapped in the gap. The temperature decay as a function of time at the interface can be modeled simply as a Fourier diffusion boundary value problem in one dimension. The metallic driver is considered to be a thermally conducting half-space with initial temperature T_d, the shock temperature of the driver, and thermal diffusivity κ. The sample is modelled as a thermal insulator. This problem is solved by Carslaw & Jaeger (1959, p.51). The solution is

$$T(x,t) = T_d + \frac{Q}{2\rho C_V \sqrt{\pi \kappa t}} e^{-x^2/4\kappa t}, \tag{3}$$

where t is the time after impact, x is the distance of a point in the driver from the interface, Q is the quantity of heat per unit area (unknown) deposited at the interface by the closing of the gap, and ρ and C_V are the density and the specific heat at constant volume of the driver material, respectively. The time dependence of the interface temperature is

$$T_i(t) = T(0,t) = T_d + Ct^{-1/2}. \tag{4}$$

If the interface radiates as a blackbody, the observed light intensity from it (with attenuation due to the growing shocked layer) is

$$I_i(t) = f_\lambda (T_d + Ct^{-1/2}) e^{-a_s(U_s - u_p)t}. \tag{5}$$

The total light intensity observed is due to both sources (Eqns. 1 and 5)

$$I(t) = f_\lambda(T)\left[1-e^{-a_s(U_s-u_p)t}\right] + f_\lambda(T_d+Ct^{-1/2})e^{-a_s(U_s-u_p)t}. \tag{6}$$

One can easily see that for $t \gg \dfrac{1}{a_s(U_s-u_p)}$, the shocked layer is effectively an opaque blackbody, and there is no time dependence in the observed intensity. For sufficiently large a_s, this occurs at t smaller than the rise time of the pyrometer photodiode and no time dependent behavior is observed at all. This is observed in shots An1T, An7T, and An10T (Fig. 2b).

For smaller a_s, the time dependence is depicted schematically in Fig. 4, and is illustrated by the spectral radiance observed in shot An3T in Fig. 5. The contribution due to the shocked sample increases from zero, when the shock wave enters the sample, asymptotically to $f_\lambda(T)$, the intensity of a blackbody at temperature T, with a time constant $\tau = \dfrac{1}{a_s(U_s-u_p)}$. The interface contribution decreases from infinity (because of the idealized assumption that all the heat is deposited at the two-dimensional interface) to zero, with a time constant $\tau < \dfrac{1}{a_s(U_s-u_p)}$, because the source is also decaying with time. The observed light intensity is the sum which decreases asymptotically to $f_\lambda(T)$, with an effective decay time bounded above by $\dfrac{1}{a_s(U_s-u_p)}$. This is the time dependence observed in shots An2T, An3T, An5T, and An6T (Fig. 2a).

One experiment, An9T, exhibits time-dependent behavior not accounted for by this simple model. The intensity of the emitted light decreases in steps as the shock wave passes through the sample, indicating that the time-dependence is in the shock front itself, as a fluctuation in temperature, absorption coefficient, or both. This is similar to behavior observed in fused quartz shocked to the stishovite-liquid mixed phases region by Lyzenga *et al.* (1983), which they interpret as a possible rate dependent behavior due to metastability near the

phase transition pressure.

In the simple model developed above (Eq. 6), the linear absorption coefficient a_s for the shocked anorthite can be constrained by measuring the effective decay times from the oscilloscope records for the shots whose results agree with the model. The upper bound for a_s is $a_{smax} = \dfrac{1}{\tau \, (U_s - u_p)}$. These values are tabulated in Table 2. The bound on a_s is seen to be an increasing function of shock pressure.

$CaAl_2Si_2O_8$ Shock Temperatures

Temperatures were calculated from the spectral radiance data by fitting them to a Planck function, as outlined by Boslough (1983) and Boslough et al. (1984a). This was done in two ways for each experiment. First, a least squares fit is carried out in which both the temperature T and emissivity ε are independent variables. The temperatures and emissivities determined in this manner are given in Table 3, along with the standard deviation σ and the mean fractional deviation $\sigma / \bar{N}_\lambda$ of the fit (where $\bar{N}_\lambda$ is the mean measured spectral radiance). There appears to be no correlation between the shock pressure and the emissivity which gives the best fit, and in the majority of cases the best fitting emissivity is greater than unity--an unphysical situation.

Because of this discrepancy, and the fact that the model developed in the previous section implies that the observed intensity corresponds to a blackbody on the asymptote, temperatures were also calculated assuming $\varepsilon = 1.0$, and conducting a standard single variable least squares fit for T.

In four of the eight anorthite shots, the best fitting emissivities are within 10% of unity, and the goodness of the fits, as determined by the standard deviations are not significantly reduced by requiring that $\varepsilon = 1.0$. In three shots, the

best fitting emissivities are significantly greater than unity. Two of these shots, An2T and An6T, have extremely good fits, with mean fractional standard deviations of .01 and .02, respectively. However, the emissivities which give rise to these fits are 1.34 and 1.76, respectively; unphysical values which imply that the quality of the fits is fortuitous. When the inversion is carried out with an emissivity of unity for these three shots, however, the qualities of the fits are still comparable to those for the other experiments.

In one shot, (An7T), spectral radiance data was obtained at only one wavelength. The shock temperature of this shot was assumed to be the brightness temperature. This assumption is based on the close agreement between the observed spectral radiances and blackbody distributions in the other seven experiments. The temperature error for this shot was taken from the estimated error in the measured spectral radiance.

In the other seven shots, the temperature errors were determined systematically by the equation

$$\Delta T = \frac{\sigma_N}{f_T \, (T, \lambda = 600 \text{nm})}, \tag{7}$$

where σ_N is the standard deviation in spectral radiance, and $f_T(T, \lambda)$ the partial derivative of the Planck distribution function with respect to temperature. The partial derivative was evaluated at a wavelength of 600 nm, because this is near the middle of the widest wavelength range used.

The intensities used in the temperature calculations were taken from the oscilloscope records as indicated in Figs. 2 and 3. According to the simple model, the intensity of light most representative of thermal radiation from the shocked region of the sample is just before the shock wave arrives at the free surface. In all but one case, that is where the oscillograms were read. In the other case, shot An9T the shock wave begins to decay before it approaches the

free surface, apparently due to an edge rarefaction. The intensity was taken from this set of shot records just prior to the beginning of the decay of the shock wave. The spectral radiances determined in this manner are tabulated in Tables 4 and 5. Plots which show the measured spectral radiances and those calculated for the blackbody temperatures which give the best fits are illustrated in Figs. 6 and 7.

Temperatures determined by both of these methods, along with their respective emissivities, standard deviations in spectral radiance and fractional standard deviations, are summarized in Table 3. The associated pressures are determined from the measured projectile velocity, and impedance matching with a fit to the U_s-u_p data obtained in the Hugoniot experiments on anorthite glass (Boslough *et al.*, 1983). These impedance-match determined pressures are the preferred values to use when modelling the pressure-temperature Hugoniot, despite the fact that pressures were determined more directly for each shot by measuring shock-transit times. In the more direct pressure determination, projectile and shock velocity must both be measured. The precision by which the shock velocity can be measured is not as high as that of the projectile velocity measurement, and larger random errors can be introduced. In the impedance-match method, only the projectile velocity is used, which can be measured to better than ±0.2%, and a curve which is determined by a least-squares fit to the direct pressure measurements. This in effect smooths out the random errors.

Discussion

The measured shock temperatures in anorthite glass are plotted as a function of Hugoniot pressure in Fig. 8, along with pressure-temperature Hugoniot calculations based on several models. These models are the Jeanloz & Ahrens (1980) equation of state with a Dulong-Petit specific heat ($C_V = 3R$), the same

equation of state with variable specific heat, and a model in which several phase transitions occur. The latter two models can provide reasonable fits to the data. The method of Ahrens *et al.* (1969) was used to calculate shock temperatures in all cases.

The Jeanloz & Ahrens equation of state considers all states above 30 GPa on the Hugoniot of anorthite crystal to be a single high pressure phase, as found by McQueen *et al.* (1967), and fits the Hugoniot data with a third order Eulerian finite strain (Burch-Murnaghan) isentrope (Davies, 1973). The Gruneisen parameter was calculated by the pressure offset of the porous Hugoniot. The transition energy between single crystal anorthite and the metastable high pressure phase at standard conditions (E_{tr}) in this equation of state is .72 MJ/kg. This corresponds to an E_{tr} of .46 MJ/kg for anorthite glass, when the .26 MJ/kg energy difference between anorthite glass and crystal is accounted for (Robie *et al.*, 1978). Jeanloz & Ahrens (1980) considered anorthite above 2000 K to be a Debye solid in the classical limit—anorthite having a Debye temperature of 1000 K—and used the Dulong-Petit specific heat. This calculation gives reasonable agreement to the measured points below 60 GPa, but overestimates the shock temperature at higher pressure by as much as 1000 K. Clearly, the slope described by the data is less steep than the calculated slope.

In calculating shock temperatures by the method of Ahrens *et al.* (1969), the only way the theoretical T-P slope can change is to have a pressure or temperature-dependent C_V and/or phase transitions. There is ample theoretical and experimental evidence for a temperature dependent C_V in this temperature range, in departure from the Debye model of solids. A specific heat of the form

$$C_V = A + BT \tag{8}$$

is equivalent to that of Wallace (1972) for NaCl, where A=3R and $B = \Gamma_2 - 2A_2$.

Here, Γ_2 is the electronic contribution and A_2 is the first order anharmonic lattice contribution. The same form has been shown by Lyzenga *et al.* (1983) to describe shock temperature dependence on pressure for solid and liquid stishovite.

The coefficients for the best fit to the anorthite data are A = 0.92 kJ/kg K and B = 9.3×10^{-6} kJ/kg K^2. These coefficients are comparable to those determined by Lyzenga *et al.* (1983) for solid and liquid stishovite, which has approximately the same mean atomic weight per atom as anorthite, with mean values of A = .86 kJ/kgK and B = 1.17×10^{-4} kJ/kg K. B is in fact smaller for all the anorthite data taken together than for the single phases of the SiO_2 data, which indicates less temperature dependence for C_V overall.

It is probably unreasonable to expect that the anorthite undergoes no phase transition along this region of its Hugoniot, however, when one considers the complexity of its phase diagram at lower pressures, below 30 GPa (Liu, 1978), and when the behavior of simpler silicates such as SiO_2 in the same pressure range (Lyzenga *et al.*, 1983) is considered. Anorthite disproportionates to grossular, kyanite, and quartz at pressures from 3 to 15 GPa (Goldsmith, 1980; Boyd & England, 1961) and at 15 GPa the quartz transforms to stishovite along its Hugoniot (McQueen *et al.* 1963). Phase changes in grossular have been observed above 25 GPa (Liu, 1979). Hugoniot data indicate a mixed phase region in anorthite form 10 to 33 GPa (Jeanloz & Ahrens, 1980). Jeanloz & Ahrens (1980) give four candidate high-pressure phases above 33 GPa: $CaAl_2Si_2O_8$ (hollandite), CaO (B2 structure) + Al_2O_3 (corundum) + $2SiO_2$ (stishovite)--(mixed oxide assemblage), $CaAl_2O_4$ (calcium ferrite structure) + SiO_2 (stishovite), and $Ca_2Al_2SiO_7$ (sodium titanate structure) + Al_2O_3 (corundum) + $3SiO_2$ (stishovite). It is not unlikely, however, that phase transitions occur between these candidate phases, or others, above 33 GPa, or that further disproportionations or polymorphic

transitions occur in the components of the candidate assemblages. Melting is also expected to occur in this shock-pressure range.

With each phase change is associated an energy of transition, which can be expressed in terms of ΔE_{tr}, the energy difference between the metastable phases at standard conditions. The measured temperature for anorthite shocked into a mixed phase region will, if in equilibrium, lie on the coexistence curve. For anorthite shocked into a single phase regime, the measured temperature will lie $\dfrac{\Delta E_{tr}}{C_V}$ below the calculated metastable temperature of the lower phases. The slopes of the single-phase segments of the Hugoniot depend on C_V.

For constant $C_V = 3R$, at least three phase transitions (to assemblages indicated as I, II, and III in Fig. 8) are required to give a good fit to the data. If stishovite is a component of assemblage II, the highest transition--at about 4800 K--may correspond to the stishovite melting coexistence curve determined by Lyzenga et al. (1983) who found ΔE_{tr} for the stishovite to liquid transition to be about 1.6 MJ/kg. The transition at 4800 K in anorthite gives a temperature difference of about 450 K between the phases, which leads to $\Delta E_{tr} \approx .5$ MJ/ kg. The mass fraction of SiO_2 in $CaAl_2Si_2O_8$ is about .36, so if this phase transition is melting of SiO_2 only, this ΔE_{tr} corresponds to 1.4 MJ/kg in the SiO_2, which compares well with the value of Lyzenga et al. (1983).

Conclusions

When shock-temperature data are included in the description of the high-pressure phase assemblages in the system $CaAl_2Si_2O_8$, it is too complicated to be described by a single high pressure phase equation of state such as Jeanloz & Ahrens (1980). Although the shock temperature data can be roughly approximated assuming a single phase and choosing a temperature dependent model for C_V, the scatter of data around the best such single-phase curve in the

pressure-temperature plane is still significantly greater than the estimated errors in the temperature measurements. It is more reasonable to interpret the shock-temperature data by assuming that a series of phase transitions continue to occur along the Hugoniot. The data are consistent with three phase transitions--at about 55, 85, and 100 GPa--each with a transition energy of about 0.5 MJ/kg. The exact transition energies and pressures are not, however, well constrained by the data. The most realistic model would include both a temperature-dependent C_V and phase transitions. It is also possible that when melting does occur, it does so incongruently, with a compositional difference between the melt and solid. Such a transition must be treated in the context of a multi-component system, in contrast to the stishovite melting transition, for which SiO_2 can be treated as a single-component system. A possible consequence of incongruent melting would be a spreading of the mixed phase region out over a larger pressure range, and a resulting shallow slope for the Hugoniot in the pressure-temperature plane.

Success of modelling the time-dependence of the measured spectral radiances demonstrates the potential usefulness of the optical pyrometry method in studying optical properties of shocked material, in addition to measuring shock temperatures. By taking advantage of the fact that decay times of emitted light can be used to determine the absorption coefficient of the material behind the shock front, as in the case of anorthite glass, the absorption coefficient increases from about 2 to >24 mm^{-1} as a function of shock-pressure (Table 2). Future experiments can be designed to determine absorption coefficient as a function of shock-pressure, and the shock state can be further characterized in this way.

Acknowledgments

References

Ahrens, T.J., Anderson, D.L. & Ringwood, A.E., 1969. Equations of state and crystal structures of high-pressure phases of shocked silicates and oxides, *Rev. Geophys.* **7**, 667-707.

Ahrens, T.J. & O'Keefe, J.D., 1977. Equations of state and impact-induced shock-wave attenuation on the moon, *Impact and Explosion Cratering*, pp. 639-656, eds Roddy, D.J., Pepin, R.O., and Merrill, R.B., Pergamon, New York.

Ahrens, T.J. & O'Keefe, J.D., 1983. Impact of an asteroid or comet in the ocean and extinction of terrestrial life, *J. geophys. Res.*, **88**, A799-A806.

Boslough, M.B., 1983. *Shock-Wave Properties and High-Pressure Equations of State of Geophysically Important Materials*, Ph.D. Thesis, California Institute of Technology, Pasadena, CA.

Boslough, M.B. & Ahrens, T.J., 1983. Shock-melting and vaporization of anorthosite and implications for an impact-origin of the moon, *Lunar and Planetary Science XIV*, pp. 63-64, Lunar and Planetary Institute, Houston.

Boslough, M.B., Ahrens, T.J. & Mitchell, A.C., 1984a. Shock temperatures in CaO, *J. geophys. Res.*, submitted.

Boslough, M.B., Rigden, S.M. & Ahrens, T.J., 1984b. Hugoniot equation of state of anorthite glass and lunar anorthosite, *Geophys. J. R. astr. Soc.*, submitted.

Boyd, F.R. & England, J.L., 1961. Melting of silicates at high pressures, *Carnegie Inst. Wash. Year Book*, **60**, 113-125.

Carslaw, H.S. & Jaeger, J.C., 1959. *Heat Conduction in Solids*, Oxford University Press, Oxford, 510 pp.

Davies, G.F., 1973. Quasi-harmonic finite strain equations of state of solids, *J. Phys. Chem. Solids*, **34**, 1417-1429.

Goldsmith, J.R., 1980. The melting and breakdown reactions of anorthite at high pressures and temperatures, *American Mineralogist*, **65**, 272-284.

Grossman, L. & Larimer, J.W., 1974. Early chemical history of the solar system, *Rev. Geophys. Space Phys.* **12**, 71-101.

Jeanloz, R. & Ahrens, T.J., 1977. Pyroxenes and olivines: Structural implications of shock-wave data for high pressure phases, in *High-Pressure Research*, pp. 439-461, eds Manghnani, M. & Akimoto, S., Academic Press, New York.

Jeanloz, R. & Ahrens, T.J., 1980. Anorthite: Thermal equation of state to high pressures, *Geophys. J. R. astr. Soc.*, **62**, 529-549.

Jenkins, F.A. & White, H.E., 1976. *Fundamentals of Optics*, McGraw-Hill, New York, 746 pp.

Kormer, S.B., Sinitsyn, M.V., Kirillov, G.A. & Urlin, V.D., 1965. Experimental determination of temperature in shock-compressed NaCl and KCl and of their melting curves at pressures up to 700 kbar, *Sov. Phys. JETP*, **21**, 689-700.

Liu, L.-G., 1978. A new high-pressure phase of $Ca_2Al_2SiO_7$ and implications for the earth's interior, *Earth Planet. Sci. Lett.*, **40**, 401-406.

Liu, L.-G., 1979. High-pressure phase transformations in the system $CaSiO_3-Al_2O_3$, *Earth planet. Sci. Lett.*, **43**, 331-335.

Lyzenga, G.A. & Ahrens, T.J., 1979. A multi-wavelength optical pyrometer for shock compression experiments, *Rev. Sci. Instr.*, **50**, 1421-1424.

Lyzenga, G.A., Ahrens, T.J. & Mitchell, A.C., 1983. Shock temperatures of SiO_2 and their geophysical implications, *J. geophys. Res.*, **88**, 2431-2444.

McQueen, R.G., Fritz, J.N. & Marsh, S.P., 1963. On the equation of state of stishovite, *J. geophys. Res.*, **68**, 2319-2322.

McQueen, R.G., Marsh, S.P. & Fritz, J.N., 1967. Hugoniot equations of state of

twelve rocks, *J. geophys. Res.*, **72**, 4999-5036.

McQueen, R.G., Marsh, S.P., Taylor, J.W., Fritz, J.N. & Carter, W.J., 1970. The equation of state of solids from shock wave studies, in *High Velocity Impact Phenomena*, pp. 294-419, ed. Kinslow, R., Academic Press, New York.

Mitchell, A.C. & Nellis, W.J., 1981. Diagnostic system of the Lawrence Livermore National Laboratory two-stage light-gas gun, *Rev. Sci. Instr.*, **50**, 347-359.

Rice, M.H., McQueen, R.G., & Walsh, J.M., 1958. Compressibility of solids by strong shock waves, *Solid State Phys.*, **6**, 1-63.

Robie, R.A., Hemingway, B.S., & Fisher, J.R., 1978. *Thermodynamic Properties of Minerals at 298.15 K and 1 Bar (10^5 Pascals) Pressure and at Higher Temperatures*, Government Printing Office, Washington, D.C.

Ross, J.E. & Aller L.H., 1976. The chemical composition of the sun, *Science*, **26**, 1223-1229.

Turekian, K.K. & Clark, S.P., Jr., 1969. Inhomogeneous accretion model of the earth from the primitive solar nebula, *Earth planet. Sci. Lett.*, **6**, 346-348.

Urtiew, P.A. & Grover, R., 1974. Temperature deposition caused by shock interactions with material interfaces, *J. Appl. Phys.*, **45**, 140-145.

Wallace, D.C., 1972. *Thermodynamics of Crystals*, J. Wiley & Sons, New York, 484 pp.

Figure Captions

Fig. 1. Shock temperature records for $CaAl_2Si_2O_8$ glass. Signal voltage is directly proportional to the intensity of the radiated light at the wavelength of the filter. (a) An5T: P = 55 GPa, T = 2700K, λ = 750nm. Time dependence is due to combination of effects: Cooling of interface and thickening of radiating (shocked) layer. (b) An10T: P = 117 GPa, T = 5600K, λ = 600nm. Initially constant signal due to high opacity of shocked layer. Decrease in intensity just before free surface arrival due to decay of shock by edge rarefaction.

Fig. 2. Shock temperature record for shot An9T: P=85 GPa, T=4000 K, λ=750nm. Time dependence can only be explained by unsteady shock. Signal voltage is directly proportional to the intensity of the radiated light at 750nm.

Fig. 3. Transmittance spectrum of a representative sample of $CaAl_2Si_2O_8$ glass (sample An7T), measured by Cary 17 spectrophotometer. Transmittance shows negligible wavelength dependence between wavelength limits of optical pyrometers (dashed lines).

Fig. 4. Schematic of shock temperature experiment. Measured light intensity is sum of light from interface (I_i) and shocked sample layer (I_s). (a) Just after shock enters sample, light from hot interface dominates, and is not attenuated significantly by thin shocked layer. (b) I_i has decreased due to cooling of interface and thickening of attenuating layer. I_s has increased due to thickening of emitting layer. (c) Interface has cooled and is further blocked by thick shocked layer. I_s, the light intensity characteristic of the shock temperature, now dominates.

Fig. 5. Measured spectral radiance from shot An3T (P = 66 GPa, T = 3000K) at λ = 650nm. The measured time dependence can be fit by a

function of the form: $A(1-e^{-\alpha t}) + Bt^{-1/2} e^{-\alpha t}$, an approximation of equation (6), with $A = 4.3 \times 10^{11}$ WSr^{-1}m^{-3}, $B = 8.2 \times 10^{12}$ WSr^{-1}m^{-3}, and $\alpha = 8.0 \times 10^{-3}$ns^{-1}.

Fig. 6. Spectral radiances measured in shots An6T, An5T, and An3T with best fitting blackbody curves.

Fig. 7. Spectral radiances measured in shots An2T, An9T, An7T, An1T, and An10T with best fitting blackbody curves.

Fig. 8. Measured shock temperatures of $CaAl_2Si_2O_8$ assuming $\varepsilon = 1.0$, and four calculated pressure-temperature Hugoniots. (A) Mixed oxide model of Boslough et al. (1983). (B) Jeanloz & Ahrens (1980). (C) This study, assuming three phase transitions to high-pressure phase regimes denoted by I, II, and III, and $C_V = 3R$. (D) This study, assuming no phase transitions and $C_V = A + BT$. The lower two dashed lines are hypothetical phase transitions. The upper one is the stishovite melting curve (Lyzenga et al., 1983). Three shock temperature data by Schmitt & Ahrens (1983) are included, which exhibit heterogeneous hot spot (graybody) behavior.
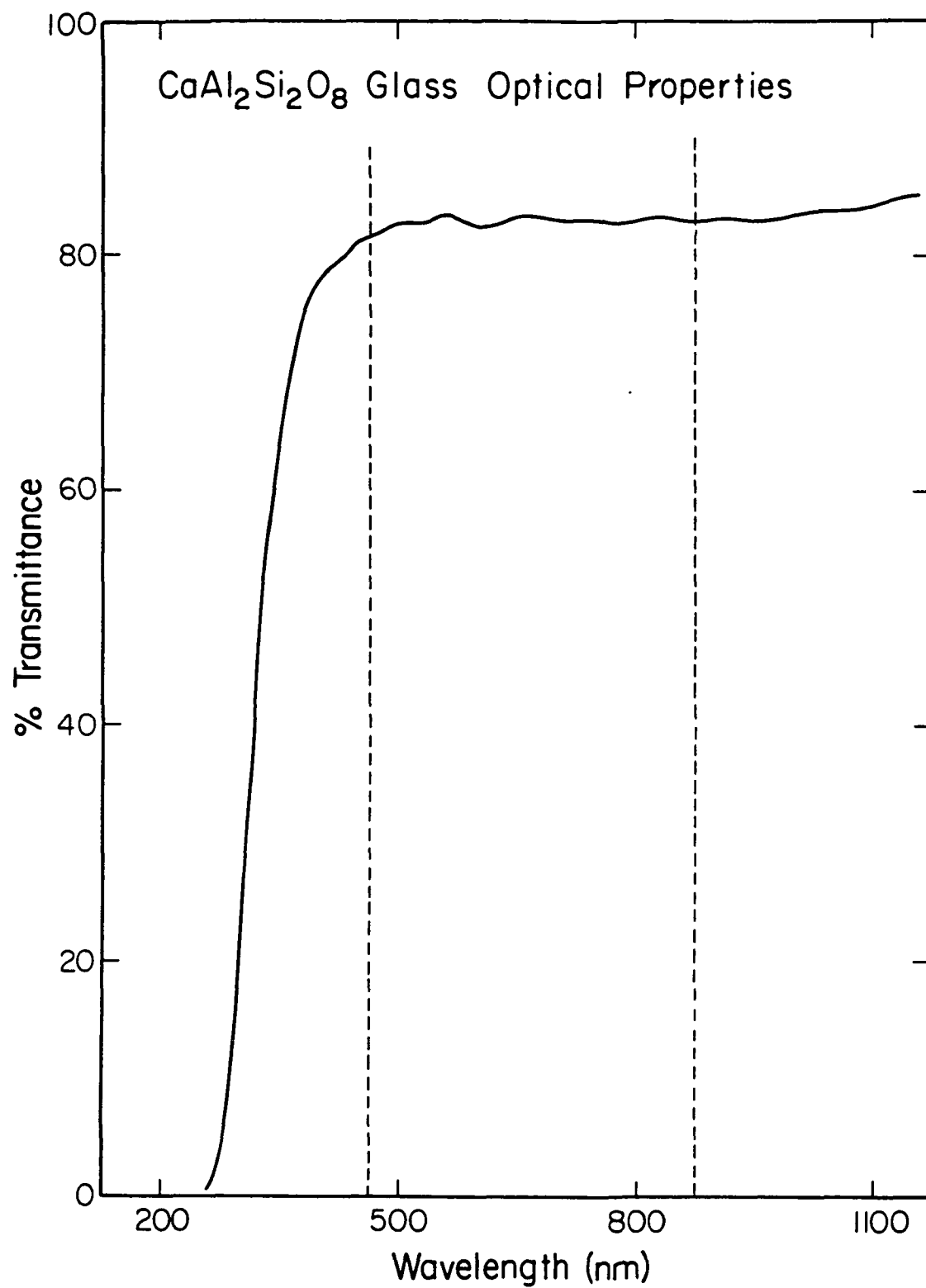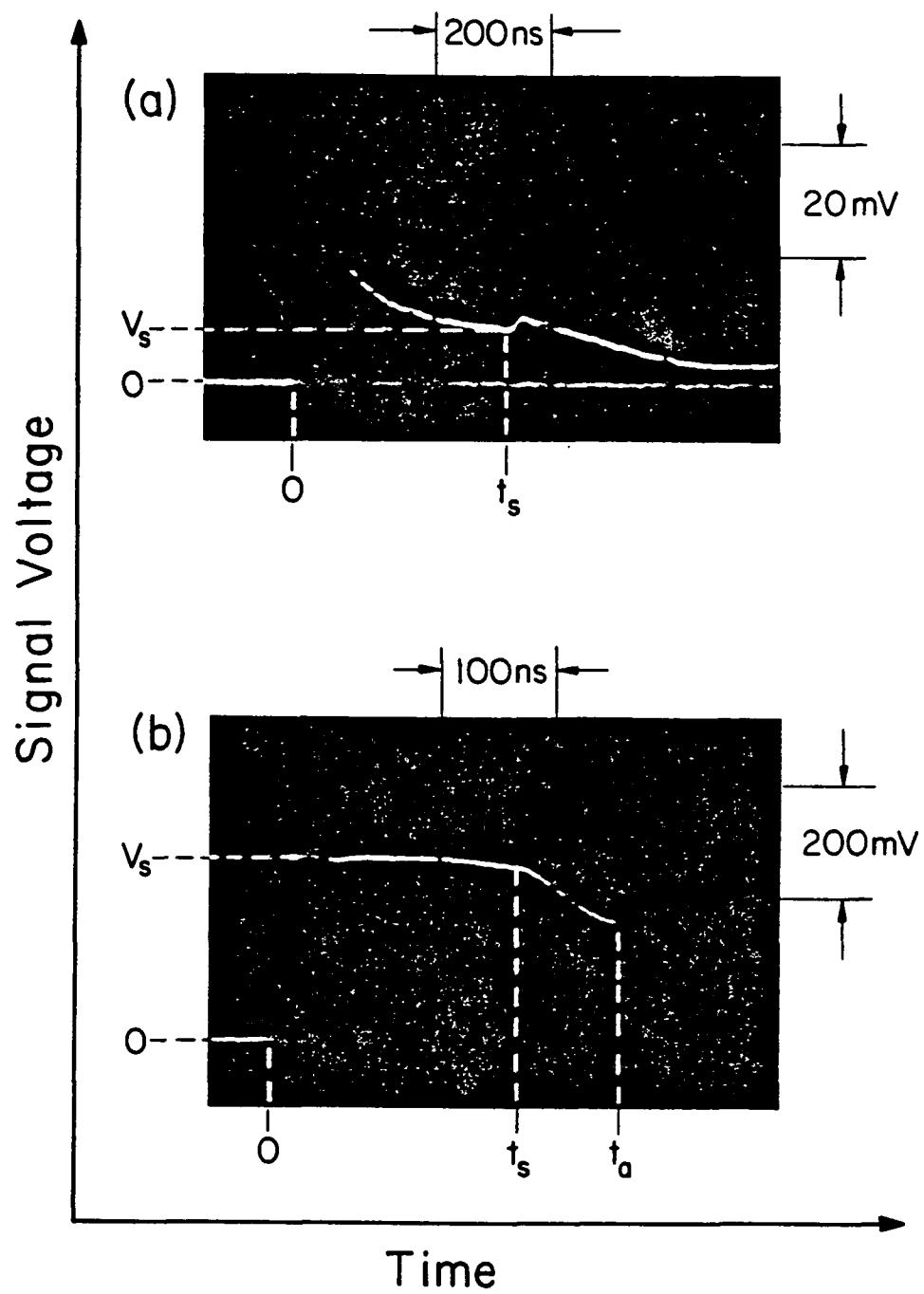
CaAl$_2$Si$_2$O$_8$ Glass Optical Properties
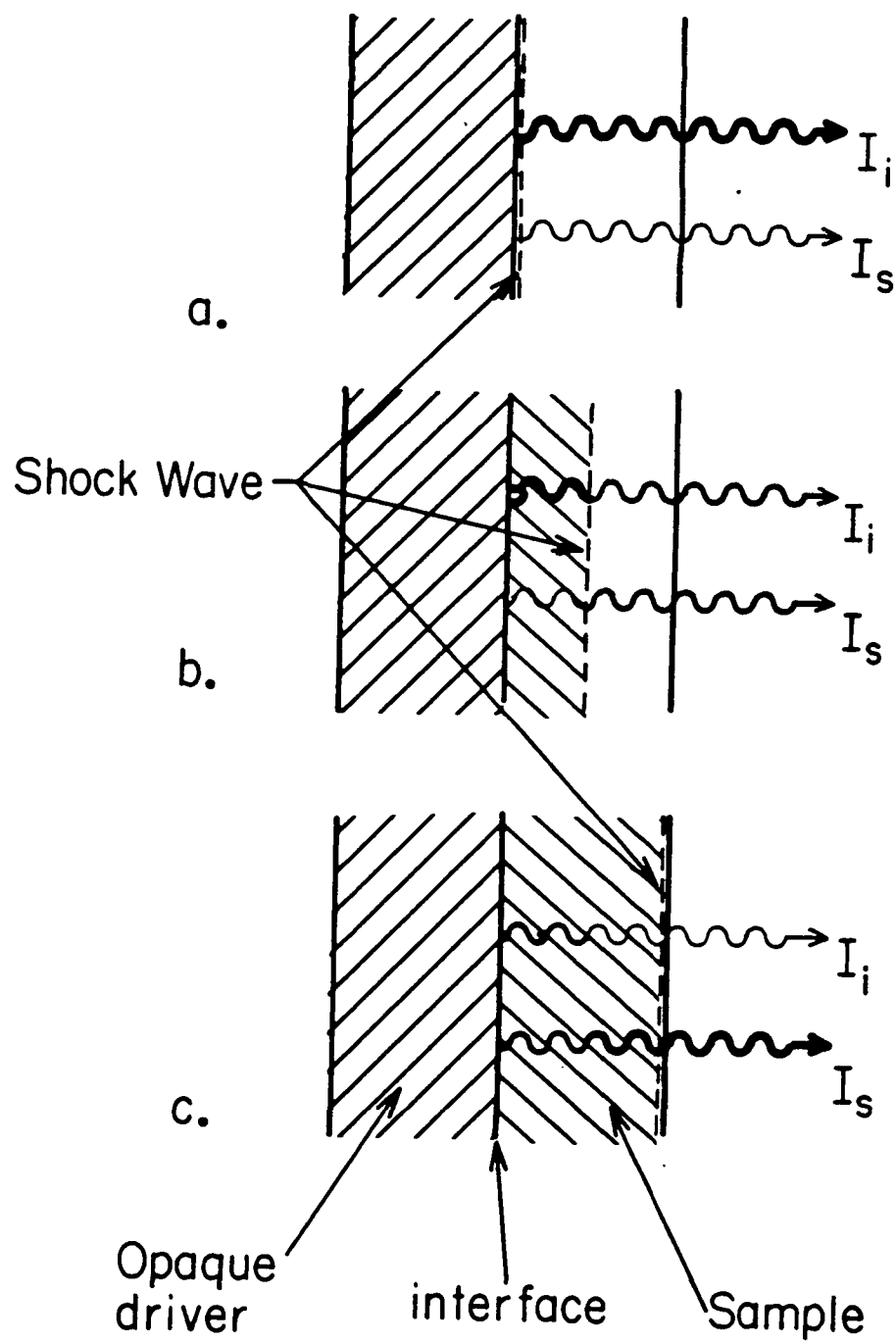
Fig. 1

TJA83107SFD

Fig. 2

a.

I_i

I_s

Shock Wave

b.

I_i

I_s

c.

I_i

I_s

Opaque
driver

interface

Sample

TJA83108SFD

Fig. 4

CaAl₂Si₂O₈ Glass
Shot An3T 650 nm

TJA83109SFD

Fig. 5

TJA84018SFD

TJA84019SFD

TJA83119SFD
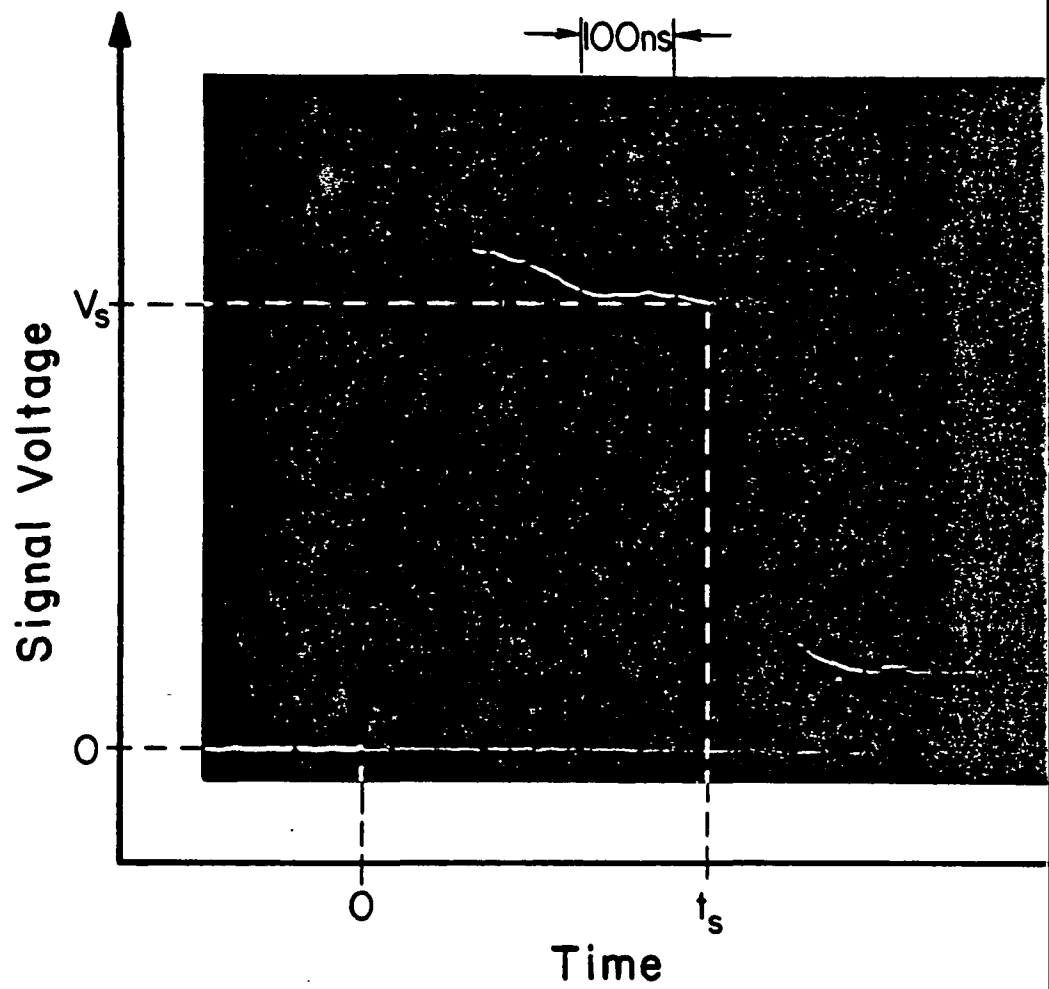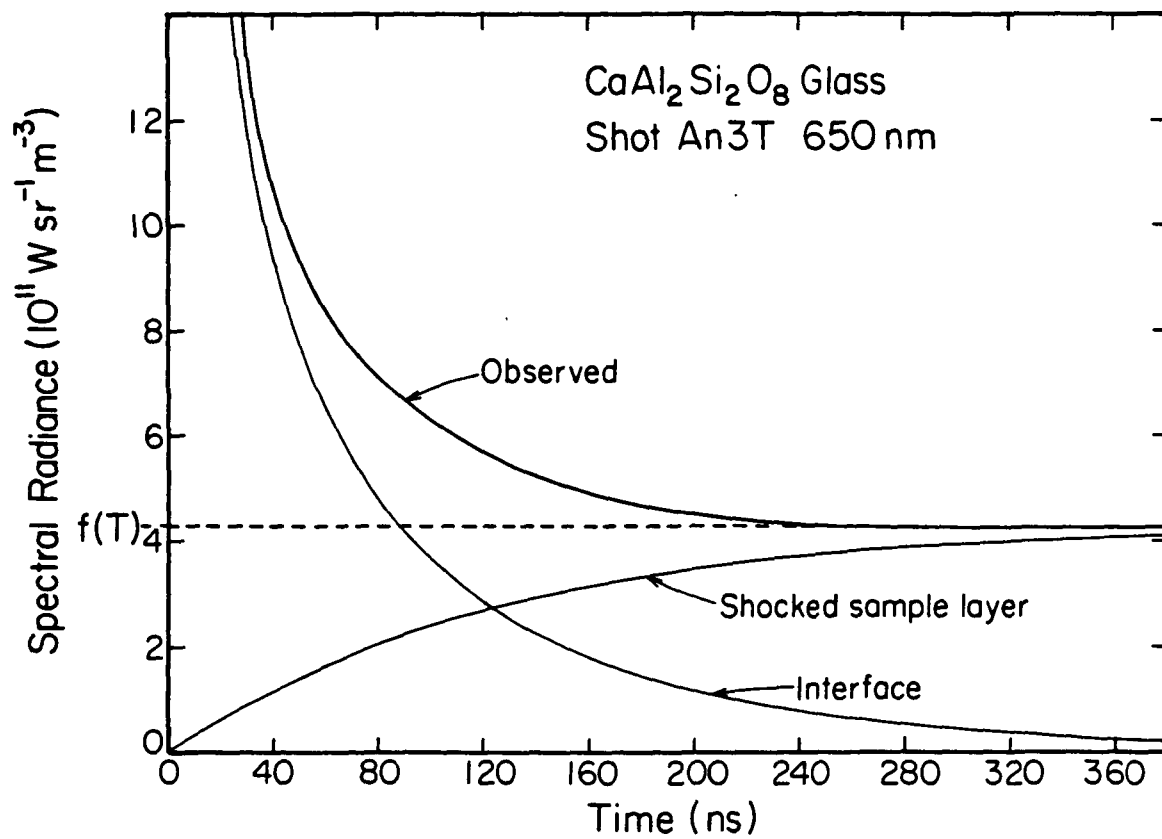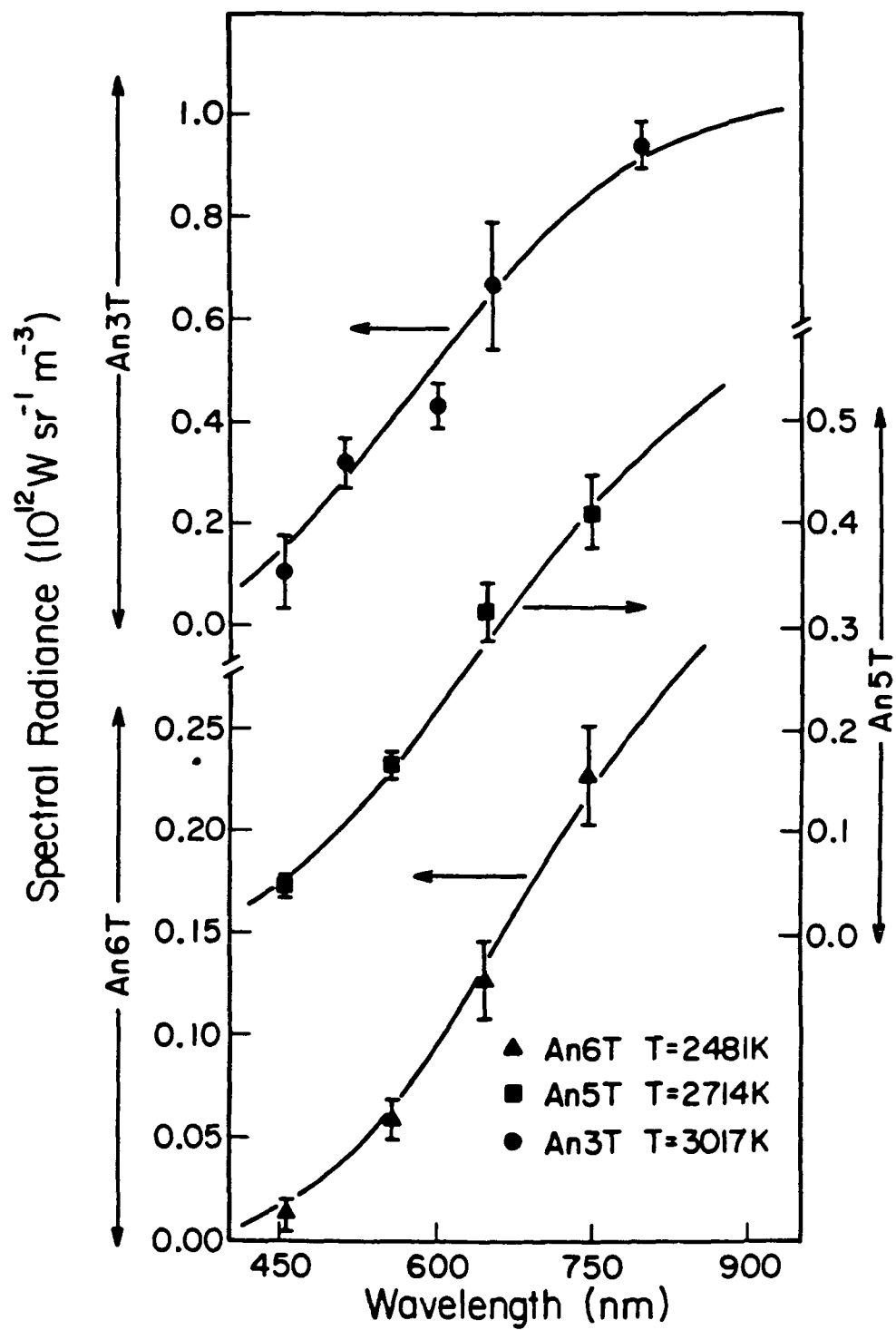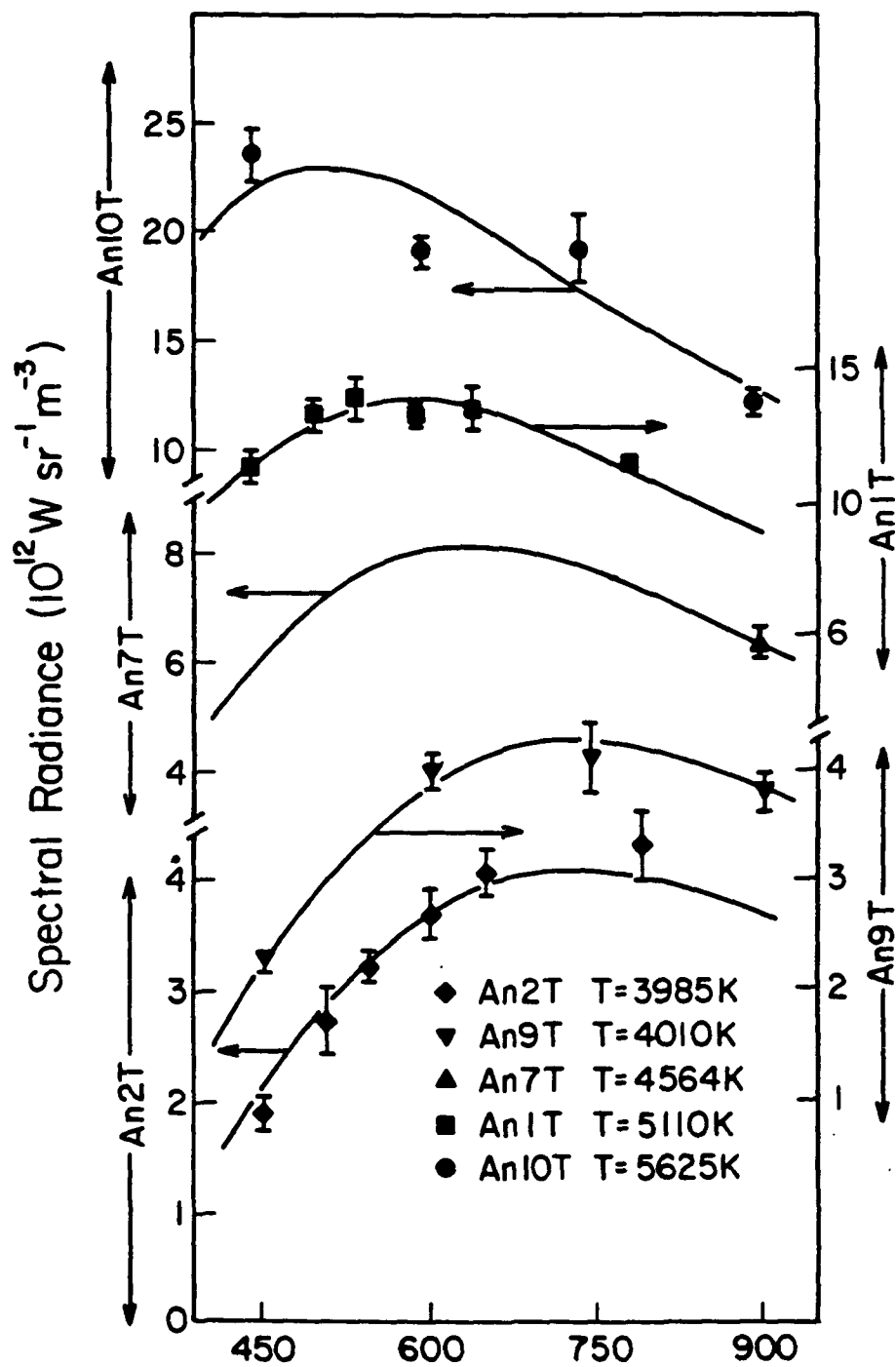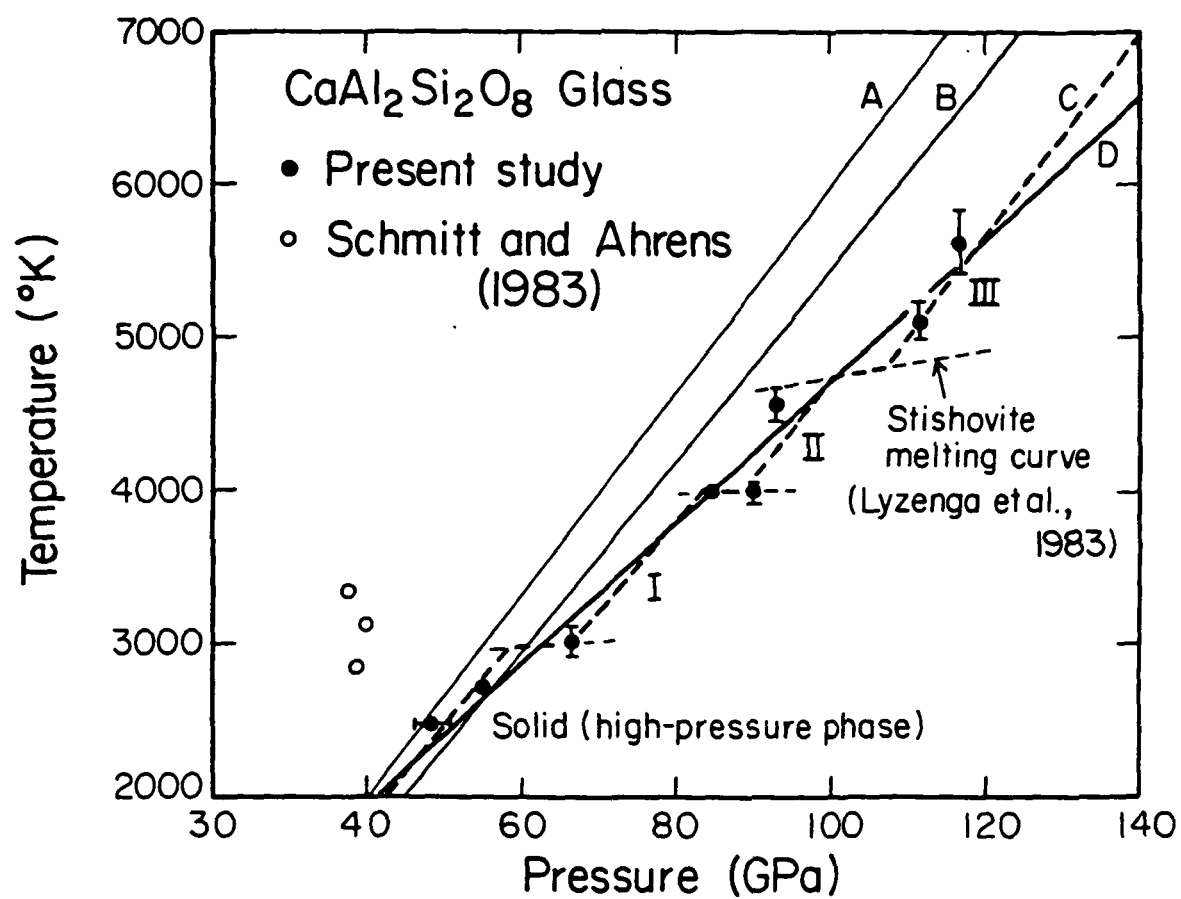
Table 1

Electron microprobe analysis of anorthite glass (Corning)

Oxide	Wt.%
Na_2O	0.05
MgO	0.00
Al_2O_3	36.36
SiO_2	43.48
K_2O	0.01
CaO	20.73
TiO_2	0.06
FeO	0.04
BaO	0.03
Total	100.76

Table 2

Bounds on absorptivity of shocked anorthite glass

Shot	τ (μs)	U_s-U_p (mm/μs)	a_{smax} (mm^{-1})	Pressure (GPa)
An6T	0.15	3.8	1.8	50.3
An5T	0.10	4.1	2.4	57.0
An3T	0.08	4.5	2.8	68.2
An2T	0.01	4.7	21	90.4
Others	<0.007	<6.	>24	>93.1

$$a_{smax} = \frac{1}{\tau(U_s-U_p)}$$

Table 3

Anorthite Glass Shock Temperature Data

Shot	Flyer/ Driver Material	Projectile Velocity (km/sec)	Initial Density (Mg/m^3)	Pressure (GPa)	Temperature Calculation				
					Method	ε	T (°K)	σ (W/sr m^3)	σ/N_λ
An6T	Cu/Cu	3.72 ±.10	2.6908 ±.0010	48.3 ±2.2	(a)	1.76	2323 ±5	0.2 ×10^{10}	0.02
					(b)	1.00	2481 ±37	1.4 ×10^{10}	0.13
An5T	Cu/Cu	4.038 ±.002	2.6909 ±.0013	55.0 ±1.1	(a)	0.98	2723 ±37	2.7 ×10^{10}	0.12
					(b)	1.00	2714 ±39	2.8 ×10^{10}	0.12
An3T	Cu/Cu	4.536 ±.006	2.6900 ±.0010	66.4 ±1.2	(a)	1.05	2997 ±104	1.5 ×10^{11}	0.30
					(b)	1.00	3017 ±105	1.5 ×10^{11}	0.30
An9T	Cu/Cu	5.255 ±.003	2.6953 ±.0012	84.5 ±1.3	(a)	1.01	4002 ±21	1.2 ×10^{11}	0.03
					(b)	1.00	4010 ±22	1.3 ×10^{11}	0.04
An2T	Cu/Cu	5.455 ±.010	2.6899 ±.0011	89.9 ±1.3	(a)	1.34	3802 ±6	0.4 ×10^{11}	0.01
					(b)	1.00	3985 ±71	4.0 ×10^{11}	0.12
An7T	Cu/Cu	5.563 ±.006	2.6927 ±.0011	92.9 ±1.2	(c)	1.00	4564 ±104		
An1T	Ta/Ta	5.678 ±.010	2.6893 ±.0011	111.5 ±1.3	(a)	1.24	4904 ±78	1.1 ×10^{12}	0.08
					(b)	1.00	5110 ±122	1.6 ×10^{12}	0.12
An10T	Ta/Cu	5.562 ±.003	2.6944 ±.0012	116.8 ±1.1	(a)	0.91	5741 ±218	3.5 ×10^{12}	0.19
					(b)	1.00	5625 ±214	3.6 ×10^{12}	0.20

(a): best fit with Planck function and variable ε

(b): best fit with Planck function and $\varepsilon \equiv 1$ (blackbody)

(c): brightness temperature

Table 4
Anorthite glass spectral radiance data

$\lambda^{(1)}$	An1T $N_{\lambda}^{(2)}$	An2T N_{λ}	An3T N_{λ}
450.2	11.4 ± 0.6	1.92 ± 0.15	0.109 ± 0.070
507.9	13.3 ± 0.5	2.73 ± 0.29	0.327 ± 0.049
545.1	14.9 ± 0.8	3.24 ± 0.13	0.489 ± 0.094
598.0	14.3 ± 0.4	3.72 ± 0.23	0.433 ± 0.044
650.0	14.5 ± 0.7	4.09 ± 0.21	0.670 ± 0.123
792.0	11.5 ± 0.3	4.34 ± 0.32	0.951 ± 0.044

1. Wavelength (λ) in nm.
2. Spectral radiance (N_{λ}) in 10^{12} $Wm^{-3}Sr^{-1}$.

Table 5

Anorthite glass spectral radiance data

An5T		An6T		An7T		An9T		An10T	
$\lambda^{(1)}$	$N_\lambda^{(2)}$	λ	N_λ	λ	N_λ	λ	N_λ	λ	N_λ
454.4	0.0455 ± 0.0078	454.8	0.0137 ± 0.0076	off scale		453.5	2.18 ± 0.09	453.0	23.5 ± 1.2
556.8	0.165 ± 0.014	557.2	0.0595 ± 0.0105	off scale		603.2	3.98 ± 0.14	602.8	19.0 ± 0.7
647.6	0.314 ± 0.028	647.6	0.0128 ± 0.019	off scale		747.5	4.25 ± 0.15	747.3	19.0 ± 1.6
748.3	0.412 ± 0.036	748.4	0.0228 ± 0.024	903.3	0.623 ± 0.026	903.3	3.77 ± 0.17	903.3	11.9 ± 0.5

1. Wavelength (λ) in nm.
2. Spectral radiance (N_λ) in 10^{12} Wm^{-3}Sr^{-1}.